$1/f$ model for long-time memory of the ocean surface temperature

Klaus Fraedrich,* Ute Luksch, and Richard Blender
Meteorologisches Institut, Universität Hamburg, Bundesstrasse 55, D-20146 Hamburg, Germany
(Received 27 August 2003; revised manuscript received 3 February 2004; published 16 September 2004)

The $1/f$ spectrum of the ocean surface temperature in the Atlantic and Pacific midlatitudes is explained by a simple vertical diffusion model with a shallow mixed layer on top of a deep ocean. The model is forced at the air-sea interface with the total surface heat flux from a 1000 year climate simulation. The analysis reveals the role of ocean advection and substantiates estimates of internal thermal diffusivities.

DOI: 10.1103/PhysRevE.70.037301 PACS number(s): 92.70.Gt, 89.75.Da, 05.40.−a, 92.70.Jw

Spectra of observed ocean surface temperatures follow $1/f$ (or flicker noise) beyond one year in northern and southern midlatitudes [1,2]. Long-term climate simulations with complex ocean models reproduce the available observations [1,3], where, apart from the North Pacific and the tropics, $1/f$ scaling occurs up to 100 yr. The long-time memory is relevant for the observed climate variability and the assessment of future anthropogenic impacts. There are various theoretical explanations for $1/f$ spectra, for example, self-organised criticality [4], correlated point processes [5], broad distributions of relaxation times [6], or forced diffusion [7]; see [8] for a review. In the present context, diffusion models are the most promising: While white stochastic volume forcing yields $f^{-1/2}$ spectra [9], the two-layer extension of van Vliet *et al.* [10] with white surface forcing leads to a $1/f$ range for the surface variability.

The aim of this Brief Report is to demonstrate that ocean surface temperature spectra in several areas in the midlatitude Atlantic and Pacific can be reproduced by a two-layer heat diffusion model [10]. The upper layer corresponds to the shallow mixed layer on top of a deep ocean. The theoretical model represents a vertical column which is forced by a stochastic atmospheric heat flux at the air-sea interface, neglecting interior horizontal processes. The model is assessed in four ocean basins where the parameters for the surface heat flux are derived from a 1000 yr simulation supplying a comprehensive and consistent data set, which is not available from observations. For the present application, which requires the calculation of first and second moments, we assume that the simulated time series become stationary on centennial time scales, although some show nonstationarity up to 1000 yr.

The temperature fluctuations in a vertical column are described by a diffusive two-layer model responding to stochastic surface forcing (see Fig. 1) [10]. Volume forcing is not considered here, since this is most intense in the mixed layer (ML) and, after vertical averaging, equivalent to surface forcing. The depth h_1 of the shallow ML is fixed to the observed global annual mean of roughly 50 m [11]. For simplicity, the deep ocean (DO) depth h_2 is fixed at 5000 m.

The fluctuations about the equilibrium overturning circulation are considered with heat anomalies diffusing according to

$$\frac{\partial T_n}{\partial t} + \frac{\partial F_n}{\partial z} = 0,\ F_n = -K_n \frac{\partial T_n}{\partial z}, \tag{1}$$

where T_n is the temperature anomaly, $c_p \rho F_n$ the heat flux anomaly, and K_1 and K_2 the thermal diffusivities in the layers $n=1,2$; c_p is the heat capacity and ρ the constant density of sea water.

In the ML, vertical diffusion is a standard approximation for turbulent exchange. Typical mixing time scales are of the order of days, hence we set $K_1 = 10^{-2}$ m^2/s. In the DO, Munk and Wunsch [12] propose vertical diffusion as an aggregation of small scale (<1 m) vertical exchange processes forced by winds and tides. They favor the global mean $K_2 = 10^{-4}$ m^2/s and report on measurements as low as $K_2 = 10^{-5}$ m^2/s, compatible with time scales of hundreds of years. The estimation of K_2 is of decisive relevance for the global ocean circulation, chemical cycles, and climate modeling [13]. Within the present study, all parameters are kept constant, except the diffusivity K_2, which is varied for the ocean basins.

The upper boundary condition in $z=0$ relates the heat flux anomaly F_0 to the ocean surface temperature $T_0 = T(z=0)$ and a stochastic forcing $\zeta(t)$,

$$F_0 = -gT_0 + \zeta. \tag{2}$$

In contrast to the setup in [10], where the surface heat flux is restricted to linearized blackbody radiation, the flux F_0 is proportional to the total heat flux across the atmosphere-ocean boundary, including solar and terrestrial radiation and sensible and latent heat fluxes (note that F, ζ, and g are normalized by the constant $c_p\rho$ compared to [10]). For a

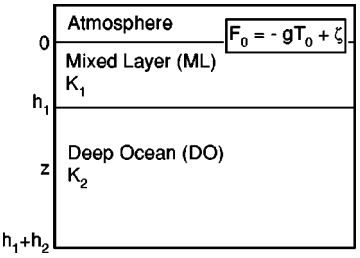

FIG. 1. Vertical structure of the diffusion model for a mixed layer and deep ocean with depths h_1, h_2 and thermal diffusivities K_1, K_2.

*Electronic address: fraedrich@dkrz.de

physical discussion of these fluxes and the linearization see [14]. The heat transfer conductance g is determined according to Eq. (2) by linear regression of F_0 with T_0, the uncorrelated residuum representing the stochastic flux ζ (the magnitude of g is 10^{-6} m/s). The variability due to horizontal advection is included in ζ. At the intermediate boundary at $z=h_1$, temperature and flux are continuous and at the lower boundary $z=h_1+h_2$ the flux vanishes.

The spectrum of the average temperature in the ML is $S_1(\omega)=S_\zeta(\omega)|R(\omega)|^2/g^2$ where $S_\zeta(\omega)$ is the spectrum of ζ and $R(\omega)$ the response function [10]

$$R(\omega)=\frac{1}{\phi_1}\left[\tanh\phi_1+\sqrt{\frac{K_2}{K_1}}\tanh\phi_2\frac{\cosh\phi_1-1}{\cosh\phi_1}\right]\times\left[\left(\tanh\phi_1+\frac{K_1}{L_1 g}\right)\sqrt{\frac{K_2}{K_1}}\tanh\phi_2+1+\frac{K_1}{L_1 g}\tanh\phi_1\right]^{-1} \quad (3)$$

with $\phi_n=h_n/L_n$ and $L_n=\sqrt{K_n/i\omega}$, for $n=1,2$. The response function is characterized by the frequencies

$$\omega_0=g/h_1,\ \omega_{00}=g/(h_1+h_2),\ \omega_1=K_2/h_2^2,\quad \omega_2=K_2/h_1^2,\ \omega_3=g^2/K_2, \quad (4)$$

which are independent of K_1. A deep lower layer, $h_2\gg h_1$, leads to $S_1\sim\omega^{-1}$ in a frequency range $\omega_3-\omega_2$ for white noise ζ. Figure 2 (similar to Fig. 2 in [10]) indicates the schematic response for parameter values relevant in the present study. The coupling of the two layers opens a new scaling regime in $\omega_3-\omega_2$, if this interval is sufficiently wide. For the observed conductance g and diffusivities K_2, both the Lorentzian and the $1/f$ range may occur.

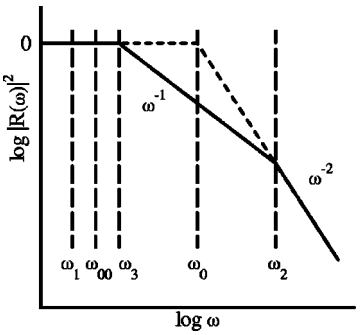

FIG. 2. Sketch of the response $|R(\omega)|^2$ according to Eq. (3) for present magnitudes of h_1, h_2, and g; ω_2 and ω_3 depend on the diffusivity K_2. The range $\omega_1-\omega_{00}$ is simplified.

The theoretical model is tested comparing its response function (3) with $|R|^2=g^2S_1/S_\zeta$ obtained from the simulation of the complex global atmosphere-ocean circulation model ECHAM4/HOPE [15] [following Fraedrich and Blender (FB) [1]]. Using a circulation model for comparison has the major advantage that the surface temperatures and heat fluxes are available, which have not been measured for sufficiently long times. The atmospheric model ECHAM4 with horizontal resolution $3.75°\times3.75°$ and 19 vertical levels describes the atmospheric dynamics, radiation, hydrological cycle, land surface, and soil. The ocean model HOPE uses horizontal resolution $2.8°\times2.8°$ and 20 vertical levels. It includes sea ice dynamics, the thermohaline circulation, and global ocean transports. The coupled ECHAM4/HOPE simulation is performed for 1000 yr under present-day climate conditions. This coupled model simulates the geographical distribution of the observed long-time memory (FB) and the long duration reveals an estimate for the uncertainty of power-law exponents in the range up to decades.

The theoretical response function (3) is compared with the

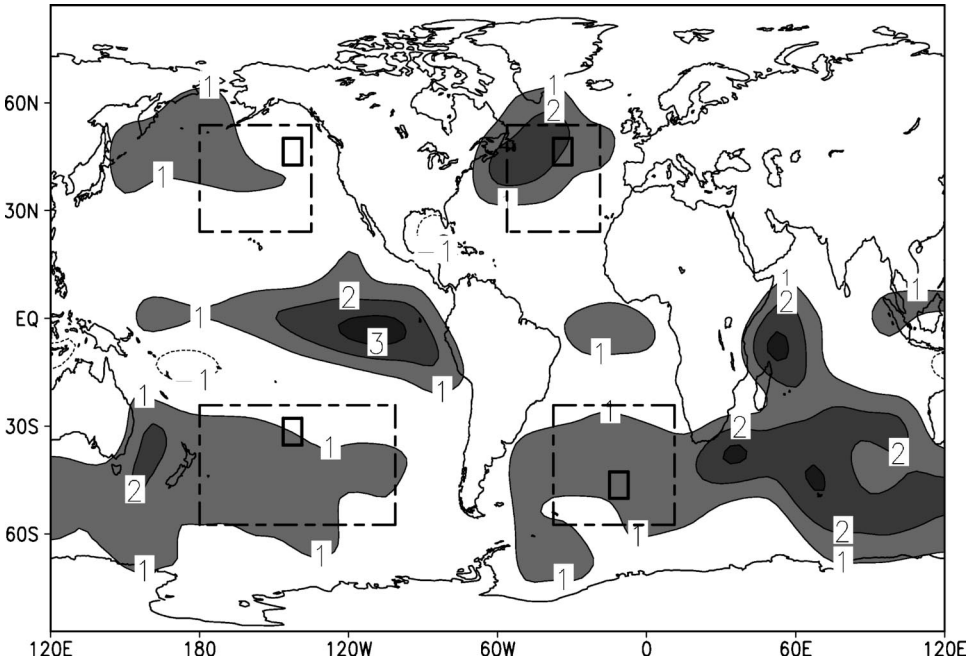

FIG. 3. Heat transfer conductance g (10^{-6} m/s) in Eq. (2) and the considered areas.

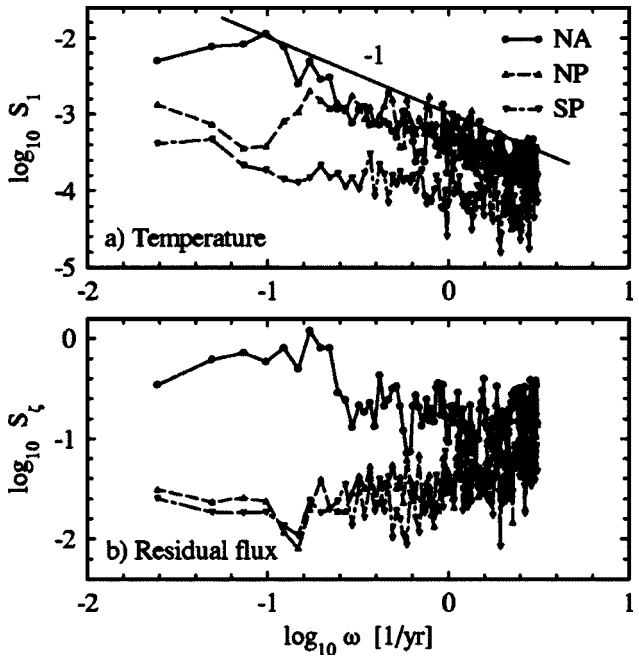

FIG. 4. Temperature spectra S_1 (a) and residual noise spectra S_ζ (b) for the North Atlantic (NA), North Pacific (NP), and South Pacific (SP) as indicated; the slope −1 is a guide.

simulated response averaged in areas of different extent, which are representative for the ocean basins (Fig. 3). Results are presented for $10° \times 10°$ areas (solid boxes of 3×3 grid points) in the North Atlantic (35°W,47°N), North Pacific (143°W,47°N), and South Pacific (143°W,31°S). For the remaining areas, including the South Atlantic and the dashed boxes, the results are briefly mentioned. The variability in these areas shows a $1/f$ spectrum up to centennial time scales, besides the North Pacific, where the spectrum is white beyond 15 yr (Fig. 3 of FB). The three areas differ with respect to the horizontal advection, which is small in the North and South Pacific, whereas higher values are observed in the North Atlantic [16]. Annual means are considered to exclude seasonal variability. All spectra used are averages of spectra in six overlapping segments (256 yr) of the 1000 yr time series.

Figure 3 displays the global distribution of the conductance g. In small areas with $g<0$ the incoming solar radiation dominates the total heat flux. The conductance is large in the northern and southern midlatitudes as well as in the tropical eastern Pacific. The temperature spectra S_1 for the three areas North Atlantic, North Pacific, and South Pacific in Fig. 4 show a $1/f$ spectrum which, in the North Pacific, is restricted to decades. The spectra S_ζ of the residual fluxes are approximately white in the North and South Pacific, whereas it shows high values of low-frequency variability in the North Atlantic. We associate this increase with advective processes in the ocean [17] since the uncoupled atmosphere is unable to yield long-time memory (FB). Therefore, as the flux spectra are not white, we use the response function $|R(\omega)|^2$ for a direct comparison with the theoretical model (3). Although the spectra are six-segment averages, they fluctuate, in particular at low frequencies. A source of uncertainty is the linear regression, because g and ζ determine the response $|R(\omega)|^2$. The response functions in the three ocean areas are presented for different diffusivities K_2.

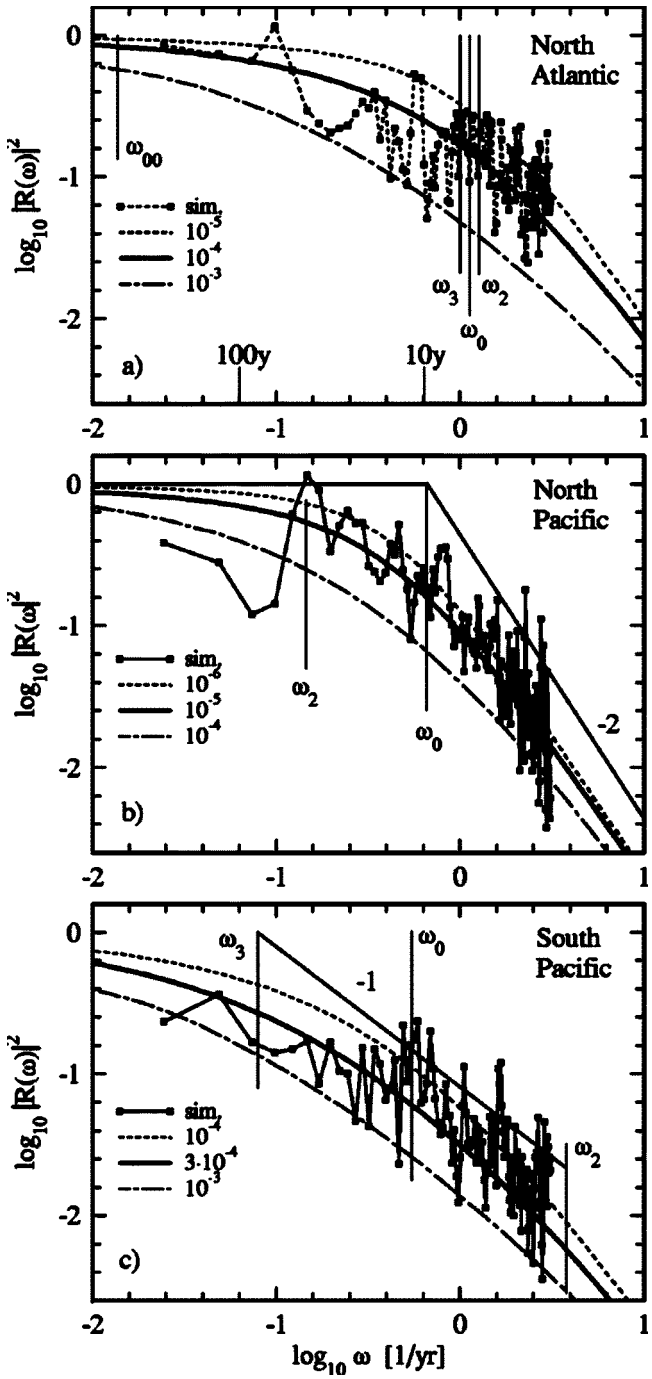

FIG. 5. Response $|R(\omega)|^2$ for (a) the North Atlantic, (b) the North Pacific, and (c) the South Pacific area. The simulations (□) are compared with the theoretical model Eq. (3) for the diffusivities K_2 (m^2/s) as indicated. Slopes −2 (b) and −1 (c) are marked. Frequencies in Eq. (4) refer to the solid curves.

The North Atlantic affected by Arctic inflow is a source of the deep thermohaline circulation. The heat transfer conductance in this area is $g=1.8\times10^{-6}$ m/s. Figure 5(a) compares the simulated response spectrum $|R(\omega)|^2$ with the theoretical spectrum (3) obtained for the global mean diffusivity K_2

$=10^{-4}$ m^2/s, the measured lower limit 10^{-5}, and a hypothetical upper limit 10^{-3}. Clearly, a close match is attained for the global mean and both other values can be excluded. The frequencies (4) identify the spectral scaling ranges for the mean diffusivity $K_2=10^{-4}$ m^2/s. A well defined $1/f$ range is absent since $\omega_3 \approx \omega_2$ with a time scale of several years. As the $1/f$ spectrum of the temperature [Fig. 4(a)] is not produced by the response $|R(\omega)|^2$ but by the residual flux spectrum [Fig. 4(b)], the observed North Atlantic $1/f$ temperature variability at decadal time scales may represent a transition phenomenon according to the local diffusion model. Since long-time memory is attributed to the ocean, we conclude that $1/f$ behavior beyond decades is a result of horizontal advection in this area.

In the North Pacific the conductance is $g=0.7 \times 10^{-6}$ m/s. The response is presented for the diffusivities $K_2=10^{-6}$, 10^{-5}, and 10^{-4} m^2/s [Fig. 5(b)]. The result for the response shows best agreement for the lower value $K_2 =10^{-5}$ m^2/s [12]. There is no $1/f$ range since $\omega_2 < \omega_0$ [see the frequencies (4)]. The spectrum is Lorentzian with ω^{-2} for large frequencies.

In the South Pacific the conductance is $g=0.9 \times 10^{-6}$ m/s. The result for the response spectrum [Fig. 5(c)] is compared to Eq. (3) for three values $K_2=10^{-4}$, 3×10^{-4}, and 10^{-3} m^2/s. Obviously, the result is rather sensitive to the choice of the diffusivity and favors the intermediate value with the frequencies (4). In this area, a $1/f$ range emerges within $\omega_3-\omega_2$ (roughly 1–100 yr). In contrast to the North Atlantic, the low-frequency $1/f$ spectrum in the South Pacific is caused by local vertical diffusion.

In the South Atlantic a comparable agreement with a smaller $1/f$ range is achieved for the diffusivity $K_2 =10^{-5}$ m^2/s (not shown). In all four basin-wide areas (dashed boxes in Fig. 3) the results agree with those in the smaller areas (solid). The South Pacific basin, however, tends to the slightly lower value $K_2=10^{-4}$ m^2/s. In the Indian and the Southern oceans, marked deviations are found. Whereas the origin of the deviations in the Indian ocean is not clear, the large horizontal flows in the Southern ocean are not reconcilable with the vertical diffusion model.

In summarizing, we show that a two-layer diffusion model is able to reproduce the main characteristics of the ocean surface temperature spectrum in the Atlantic and Pacific midlatitudes. The theoretical model considers vertical diffusion in two layers with different thermal diffusivities, which reflect the vertical transport processes. The model is local and neglects horizontal advective processes. At the air-sea boundary it is forced by a surface heat flux, which is split into a linear temperature dependence and a residual stochastic component, determined empirically by linear regression from a 1000 yr climate simulation of a coupled complex atmosphere-ocean model. The theoretical spectra coincide with the simulated spectra within the statistical uncertainty, if the forcing spectrum is included. The results are not sensitive to the ML diffusivity.

This analysis provides a simple explanation for the possible physical mechanism underlying the oceanic long-term memory, which is not simulated by a mixed layer ocean [1]. Given the framework of the theoretical model, estimates of large scale diffusivities (based on mean energy balance considerations [12]) are substantiated by a low-frequency fluctuation analysis. In addition, the model discriminates between the contributions of local vertical diffusion and horizontal advection. A major advantage of the present analysis is that it uses easily available surface information to derive properties of the internal ocean dynamics.

The authors thank S. Legutke, R. Voss, and E. Roeckner for providing the simulation data and F. Lunkeit, E. Meier-Reimer, P. Müller, and C. Penland for discussions. Financial support by the Deutsche Forschungsgemeinschaft is acknowledged (Grants No. SFB512 and No. FR450-1/2).

[1] K. Fraedrich and R. Blender, Phys. Rev. Lett. **90**, 108501 (2003).
[2] R. A. Monetti, S. Havlin, and A. Bunde, Physica A **320**, 581 (2003).
[3] R. Blender and K. Fraedrich, Geophys. Res. Lett. **30**(14), 1769 (2003).
[4] S. Maslov, C. Tang, and Y.-C. Zhang, Phys. Rev. Lett. **83**, 2449 (1999).
[5] B. Kaulakys and T. Meskauskas, Phys. Rev. E **58**, 7013 (1998).
[6] E. Milotti, Phys. Rev. E **51**, 3087 (1995).
[7] N. G. Van Kampen, *Stochastic Processes in Physics and Chemistry* (North-Holland, Amsterdam, 1992).
[8] M. B. Weissman, Rev. Mod. Phys. **60**, 537 (1988).
[9] J. D. Pelletier, J. Clim. **10**, 1331 (1997); J. D. Pelletier and D. L. Turcotte, Adv. Geophys. **40**, 91 (1999).
[10] K. M. van Vliet, A. van der Ziel, and R. R. Schmidt, J. Appl. Phys. **51**, 2947 (1980).
[11] S. Levitus, *Climatological Atlas of the World Ocean. Technical Report*, NOAA Professional Paper No. 13 (U.S. GPO, Washington D.C., 1982), p. 373.
[12] W. Munk and C. Wunsch, Deep-Sea Res., Part I **45**, 1977 (1998); see C. Wunsch and R. Ferrari, Annu. Rev. Fluid Mech. **36**, 281 (2004) for a review.
[13] A. Ganachaud and C. Wunsch, Nature (London) **408**, 453 (2000); D. J. Webb and N. Suginohara, *ibid.* **409**, 37 (2001); M. C. Gregg, T. B. Sanford, and D. P. Winkel, *ibid.* **422**, 513 (2003); H. L. Simmons *et al.*, Ocean Modell. **6**, 245 (2004).
[14] R. L. Haney, J. Phys. Oceanogr. **1**, 241 (1971).
[15] S. Legutke and U. Cubasch, CAS/JSC Working Group on Numerical Experimentation, Report No. 29, 2000 (unpublished).
[16] S. Legutke and E. Maier-Reimer, Deutsches Klima-Rechenzentrum, Hamburg, Technical Report No. 21, 1999 (unpublished).
[17] C. Frankignoul and R. W. Reynolds, J. Phys. Oceanogr. **13**, 1131 (1983).